

Corrosion and electrochemical behavior of Mg–Y alloys in 3.5% NaCl solution

Xin ZHANG^{1,2,3}, Yong-jun LI¹, kui ZHANG¹, Chang-shun WANG^{2,3},
Hong-wei LI^{2,3}, Ming-long MA¹, Bao-dong ZHANG^{2,3}

1. State Key Laboratory for Fabrication and Processing of Nonferrous Metals,
Beijing General Research Institute for Nonferrous Metals, Beijing 100088, China;

2. Beijing Engineering Research Center for Advanced Manufacturing and Evaluation of Special Vehicle Parts,
Beijing 100072, China;

3. Technology Institute, Beijing North Vehicle Group Corporation, Beijing 100072, China

Received 27 June 2011; accepted 14 December 2011

Abstract: The corrosion mechanism of Mg–Y alloys in 3.5% NaCl solution was investigated by electrochemical testing and SEM observation. The electrochemical results indicated that the corrosion potential of Mg–Y alloys in 3.5% NaCl solution increased with the increase of Y addition. The corrosion rate increased with the increase of Y addition because of the increase of Mg₂₄Y₅ intermetallic amounts. The corrosion gradually deteriorated with the increase of immersion time. The corrosion morphologies of the alloys were general corrosion for Mg–0.25Y and pitting corrosion for Mg–8Y and Mg–15Y, respectively. The main solid corrosion products were Mg(OH)₂ and Mg₂(OH)₃Cl·4H₂O.

Key words: Mg–Y alloy; polarization curves; pitting corrosion; corrosion products

1 Introduction

Magnesium is an attractive metal because of its low density of 1.74 g/cm³, and relatively high abundance in earth crust (2.7%) and sea water (0.13%). Magnesium alloy can be an alternative to aluminum alloy in a wide range of fields, such as aerospace, electronic, automobile industries [1–4]. However, the corrosion performance of magnesium alloy is a major obstacle to its wider structural applications, despite their high specific stiffness, good machinability, high damping capacity, castability, weldability and recyclability.

Magnesium alloy is generally combined with alloying elements to improve its corrosion performance [5–7]. It is known that the addition of rare earth is an effective way to improve the corrosion resistance of magnesium alloys, which is mainly attributed to the formation of metastable RE-containing phases along the grain boundaries and such other reasons as the melt purity, decreasing activity of the alloy surface.

Yttrium is a useful alloying element for Mg alloys. Y-containing Mg alloys having good mechanical

properties have been developed, such as WE54 [8], WE43 [9] and EW75 [10]. And these Y-containing Mg alloys also have good anti-corrosion properties. So yttrium is selected as alloying element [11,12]. Mg–Y alloys have three different intermetallic phases in different temperature ranges with increasing the content of Y, Mg₂₄Y₅, Mg₂Y and MgY [13]. Some characteristics of the mechanical properties of Y-containing Mg alloys have been studied [14,15], however, the corrosion properties of these alloys have received comparatively little attention [16–18]. MILLER et al [19] demonstrated that improved corrosion resistance of Mg–Y alloys was achieved when Y was confined to the solid solution. DAVENPORT et al [20] found that heat treatment and redistribution of the Y-rich regions in WE43 alloy could improve the corrosion resistance.

The aim of this work was to study the corrosion behaviour of three Mg–Y alloys in 3.5% NaCl solution. The effect of immersion time and Y concentration on corrosion resistance of the alloys was measured by electrochemical analysis and hydrogen evolution, scanning electron microscopy (SEM), energy dispersive X-ray spectrometry (EDS) and low-angle X-ray

diffraction (XRD).

2 Experimental

2.1 Materials

Mg–Y alloys were prepared according to the procedure designed by LI et al [21]. They were prepared in a crucible furnace under the protection of CO_2+SF_6 gases and cast in a water cooled metallic model. Pure magnesium and pure yttrium were used as raw materials.

The actual compositions of the Mg–Y alloys were determined by inductively coupled plasma-atomic emission spectrometry (ICP-AES) and the results are presented in Table 1.

Table 1 Actual composition of Mg–Y alloys

Alloy	Chemical composition/%	
	Y	Mg
Mg–0.25Y	0.24	Bal.
Mg–8Y	7.46	Bal.
Mg–15Y	13.78	Bal.

For metallographic characterization, the samples were prepared by ingot casting process. The specimens were encapsulated by epoxy resin with a surface of 10 mm×10 mm exposed to the solution. The specimens were wet ground through successive grades of silicon carbide abrasive papers from P120 to P1500 followed by diamond finishing to 2.5 μm in water, degreased with acetone, washed with deionized water, rinsed with isopropyl alcohol in an ultrasonic bath and dried in cool flowing air before tests. All tests were performed in duplicate to guarantee the reliability of the results. The etching reagent of 5 mL HNO_3+95 mL ethanol was used to reveal the constituents and general microstructure of Mg–Y alloys.

2.2 Immersion tests and products analysis

The immersion tests were conducted in the 3.5% (mass fraction) NaCl solution, which was prepared with AR grade NaCl and distilled water, at room temperature for 2 h and 24 h.

The corrosion rate was evaluated by measuring the evolved hydrogen during immersion in the 3.5% NaCl solution. The specimen was horizontally immersed in 1500 mL solution and the hydrogen evolved during the experiment was collected in a burette above the sample [22]. The corrosion rate, P (mm/a), was related to the evolved hydrogen rate, V (mL/($\text{cm}^2\cdot\text{d}$)) by [23]

$$P=2.279V \quad (1)$$

After the immersion test, the specimens were then quickly washed with distilled water and dried in warm flowing air. The samples were immersed in a 400 mL aqueous solution of 10% $\text{CrO}_3+1\%$ AgNO_3 in boiling condition for 5–8 min to remove the corrosion products. The corrosion morphologies of the samples were observed by JSM-6510A scanning electron microscope (SEM) equipped with an energy dispersive X-ray spectrometer (EDS). In order to get the corrosion products, the samples were immersed in the solution for 72 h. The corrosion products were investigated by grazing incidence X-ray diffraction using $\text{Cu K}\alpha_1$ ($\lambda=0.154056$ nm) radiation at a constant incidence angle of 1° to the specimen surface. The crystalline phases were identified using the JCPDS database cards.

2.3 Electrochemical measurements

The parameters of electrochemical measurements were obtained in 5% NaCl solution using the Potentiostat/Galvanostat Model 273A and HF Frequency Response Analyzer SI1255. A classical three-electrode cell was used with platinum as counter electrode, saturated calomel electrode SCE (0.242 V vs SHE) as reference electrode, and the sample as working electrode. The samples were mounted using epoxy resin and only left an exposed area of 1 cm^2 . The measurements began from the cathodic side at a constant voltage scan rate of 0.5 mV/s after the initial retard of 300 s. The perturbing signal of AC amplitude was 5 mV and the frequency ranged from 100 Hz to 5 MHz.

3 Results

3.1 Microstructural characterization

The microstructure of as-cast Mg–Y alloys consisted of primary α -Mg, yttrium-rich net-segregation Mg_{24}Y_5 phases, as illustrated in Fig. 1. In Mg–Y alloys, yttrium was in solid solution and precipitated in the form of second phases along grain boundaries. The yttrium gathered around grain boundaries and formed the network structures, and some casting defects were also distributed in the microstructure. There were some Mg_{24}Y_5 eutectic structures on the grain boundaries as shown in Fig. 2. Mg_{24}Y_5 particles looked like bright pearls enmeshed on the grain boundaries (Fig. 1(b)), and the amount of the intermetallic or eutectic Mg_{24}Y_5 phases increased with the increase of yttrium addition.

3.2 Hydrogen evolution

Figure 3 presents the hydrogen evolution with immersion time for Mg–Y alloys in 3.5% NaCl solution. In the initial stage, the hydrogen evolution was little. With the increase of immersion time, the corrosion rates

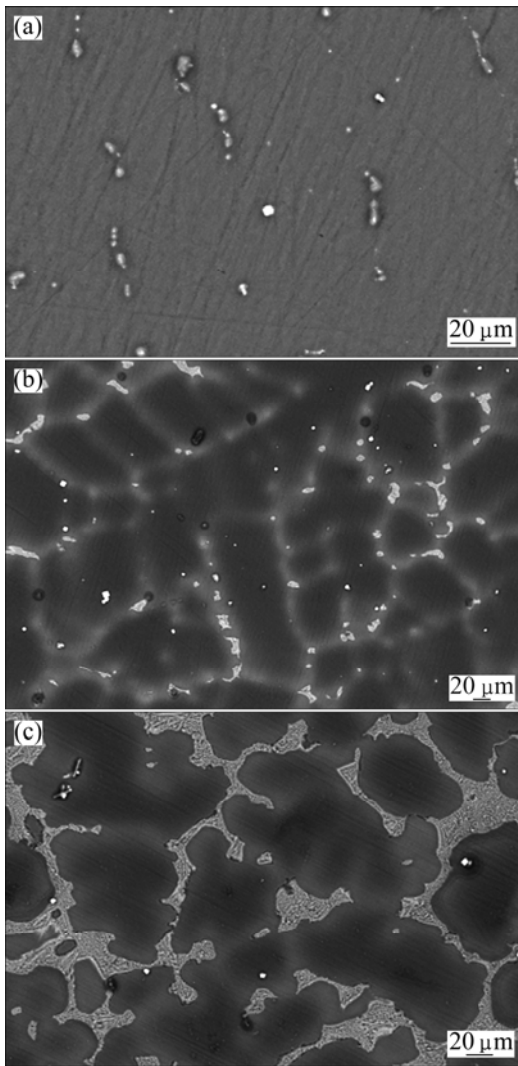


Fig. 1 Back-scattered electron images of Mg–Y alloys: (a) Mg–0.25Y; (b) Mg–8Y; (c) Mg–15Y

of Mg–8Y and Mg–15Y alloys increased remarkably, whereas the corrosion rate of Mg–0.25Y alloy increased slowly.

3.3 Characterization of corrosion morphology

The corrosion morphologies for the tested materials after immersion in 3.5% NaCl solution for 2 h are shown in Fig. 4, where the corrosion products were removed. From the corrosion morphologies, the corrosion resistance of the samples shifted negatively with the increase of yttrium addition from 0.25% to 15%, because of the formation of second phase $Mg_{24}Y_5$. The corrosion morphologies on the cross section of the samples also indicated the same results. As for Mg–0.25Y alloy, the cathodic phases consisting of $Mg_{24}Y_5$ were little and dispersed homogeneously. This can be seen from the corrosion morphology on the Mg–0.25Y surface whose corrosion was general corrosion, as shown in Fig. 4(a). With the increase of yttrium addition, the corrosion

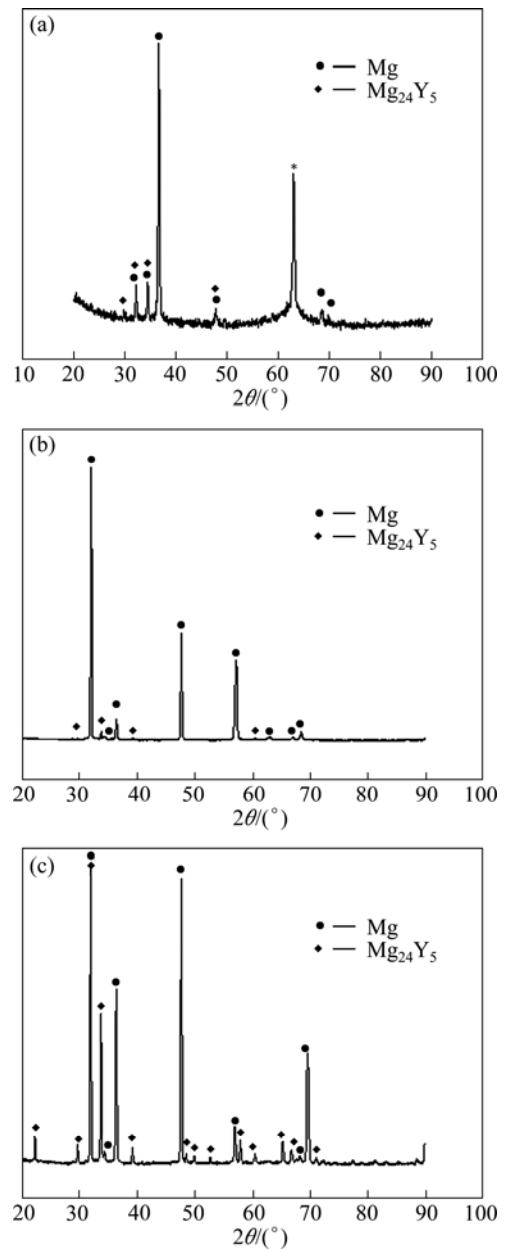


Fig. 2 XRD patterns of Mg–Y alloys: (a) Mg–0.25Y; (b) Mg–8Y; (c) Mg–15Y

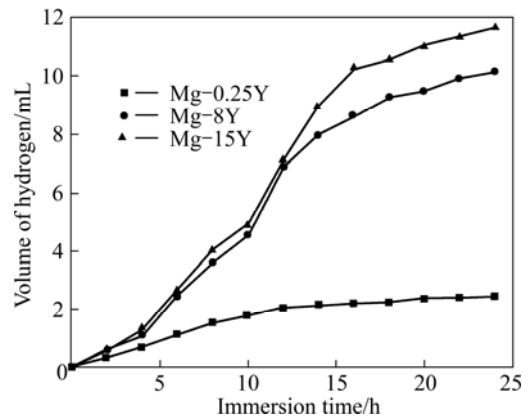


Fig. 3 Hydrogen evolution with immersion time for Mg–Y alloys immersed in 3.5% NaCl solution

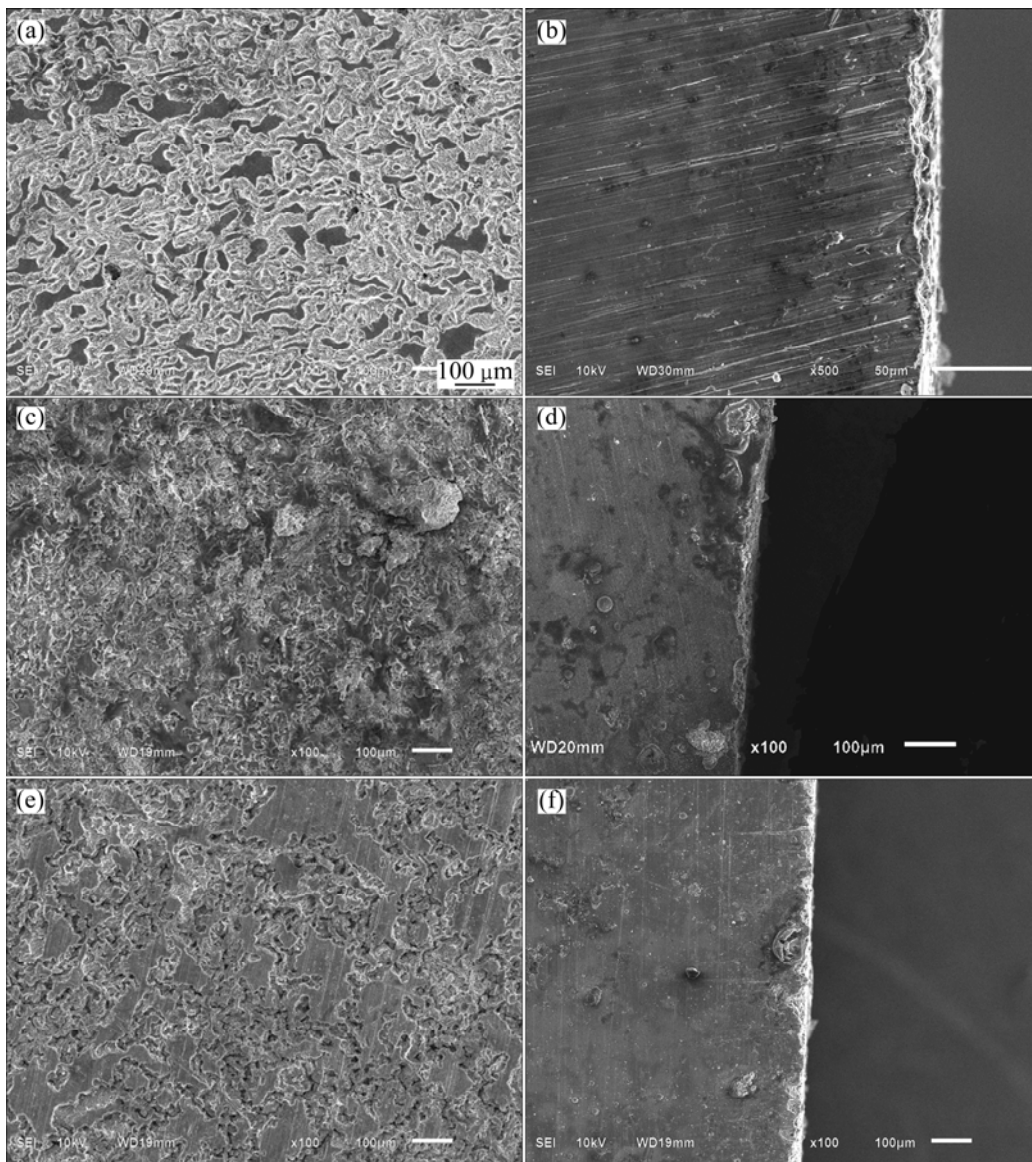


Fig. 4 SEM micrographs of alloys immersed in 3.5% NaCl solution for 2 h: (a, b) Mg–0.25Y; (c,d) Mg–8Y; (e,f) Mg–15Y

morphology changed from the general corrosion to local corrosion, with a small amount of pitting corrosion, because of the formation of bigger and homogeneously distributed cathodic phases $Mg_{24}Y_5$, as shown in Fig. 4(c). When the addition of yttrium increased up to 15%, the corrosion morphology was pitting corrosion and general corrosion, as shown in Fig. 4(e). The size and depth of the pitting corrosion for Mg–15Y were greater than those of Mg–8Y because of the increased amount of eutectic phase $Mg_{24}Y_5$. Corrosion pits nucleated on the α phase and propagated continuously. The reason should be attributed to the influence of yttrium on the second phase $Mg_{24}Y_5$, as shown in Figs. 4(a), (c) and (e). In fact, the second phase $Mg_{24}Y_5$ is an important obstacle to the propagation of corrosion pits. The more the second phase $Mg_{24}Y_5$ was isolated, the more easily the corrosion pits developed on the alloy surface. Consequently, the

refinement of the second phase $Mg_{24}Y_5$ played a positive role in suppressing the propagation of corrosion pits into the alloy matrix.

The two-phase alloy had the high corrosion susceptibility, particularly for localized corrosion because the elements in the phase boundaries unevenly distributed [24,25]. As for the Mg–0.25Y, Y element was completely dissolved into the α -Mg phase, and there was no $Mg_{24}Y_5$ phase. So, the corrosion susceptibility of the entire etching surface was relatively equal, and each point on the surface in the corrosion process might corrode [26]. So, the corrosion mechanism of Mg–0.25Y was general corrosion.

Pitting corrosion is a typical corrosion mode for the dual-phase magnesium alloys because the difference of corrosion potential can accelerate the corrosion rate of the low corrosion potential phase. Thus, the micro-

galvanic corrosion leads to the nucleation of corrosion pits on the α phase. Corrosion pits initiate on the bare α phase of the samples immersed in 3.5% NaCl aqueous solution in the initial corrosion, and also turn into the main corrosion mode judged from the corrosion morphologies. After the nucleation, corrosion pits continuously extend along the alloy surface (Figs. 4(c) and (e)), while they develop in the direction perpendicular to the alloy surface. In the NaCl solution, the gradual deterioration of surface film usually owes to the attack of Cl^- ions. The Cl^- ions preferentially attack the weak sites of the film to form the active sites. Then, the corrosion initiates at the active sites. As a result, obvious corrosion is visible for the sample as shown in Fig. 4. Cl^- ion is usually harmful to magnesium alloy [27]. CHEN et al [28] reported that Cl^- could accelerate the corrosion of magnesium alloy as it could get across the oxide and hydroxide films and reach the corrosion interface in the aqueous solution.

When the immersion time was increased up to 24 h, the corrosion morphology wholly changed into the general corrosion, and the outer surfaces were corroded out from the samples, as shown in Fig. 5. This was because with the increase of immersion time, the α phases were gradually corroded out from the surfaces of the samples, then the second phases Mg_{24}Y_5 had no sustainer to keep intact and also departed from the samples. There were some second phases embedded in the wall of the corrosion morphologies marked with the arrows shown in Fig. 5, which played an important role in decelerating the corrosion of α -Mg matrix with the increase of exposure time. Thus, the second phases would act as long-term cathodic phases to decelerate the corrosion of the samples. It was found that the α -Mg matrix surrounding the second phases was depleted due to corrosion, but the second phases still kept intact and protruded from the matrix surface. This result proved that the second phases acted as cathodes and the α -Mg matrix surrounding the second phases acted as anode during corrosion process. It can be seen that the corrosion rates derived from the corrosion morphologies increased in the following order: $\text{Mg-15Y} > \text{Mg-8Y} > \text{Mg-0.25Y}$, which could also be obtained from the observation of the cross section in Figs. 4(b), (d) and (f).

The distribution of yttrium on the surface of the samples after immersion in 3.5% NaCl solution for 2 h and removing the corrosion products is shown in Fig. 6. It was observed from Fig. 6 that the Y element mainly distributed at the grain boundaries. In addition, it was also found that the Y element homogeneously distributed in Mg-0.25Y and inhomogeneously distributed in

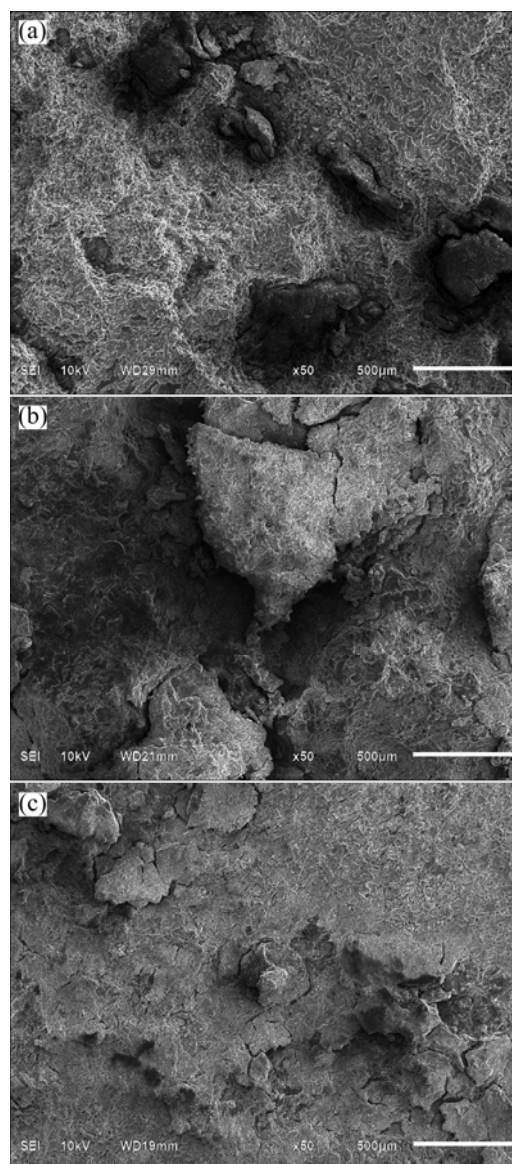


Fig. 5 SEM images of alloys immersed in 3.5% NaCl solution for 24 h: (a) Mg-0.25Y; (b) Mg-8Y; (c) Mg-15Y

Mg-8Y and Mg-15Y alloys, which was consistent with the microstructure of the original samples. Phase boundaries are the sensitive sites of corrosion due to the inhomogeneous distribution of alloying elements in two phases [29]. The corrosion of Mg-Y alloys also proved that the corrosion initiated from the boundary of α phase and Mg_{24}Y_5 phase. Then, the corrosion extended toward the more active Mg_{24}Y_5 phase. According to the classical corrosion mechanism [30], the small size of Cl^- ion could penetrate the surface oxide film to attack the magnesium substrate and then to form corrosion pits. In magnesium substrate the anodic dissolution reaction took place inside the corrosion pits. Then Mg^{2+} and Y^{n+} could induce hydrolysis reaction. The corrosion resulted in the abscission of the α phase and Mg_{24}Y_5 phase gradually, and the surface slough off from the samples

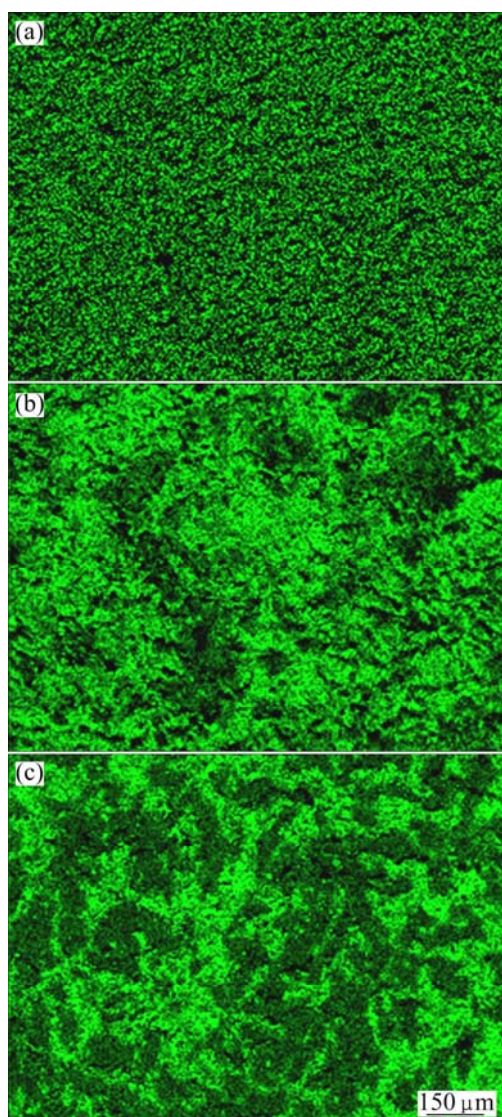


Fig. 6 Distribution of Y element on surface of Mg–Y alloys after removing corrosion products: (a) Mg–0.25Y; (b) Mg–8Y; (c) Mg–15Y

at last. So, the distribution of yttrium in the samples after corrosion was consistent with that of the original samples. However, the content of yttrium in the removed corrosion products was higher than that in the original samples, as shown in Fig. 7. This is because the $Mg_{24}Y_5$ phase has higher potential than α phase, and the quantity and area of α phase removed from the samples were greater than those of $Mg_{24}Y_5$ phase (Fig. 7). The results can be also induced from Fig. 6. In general, it is indicated that the presence of yttrium in Mg–Y alloys has a harmful effect on the corrosion behavior in chloride media. In the present work, the corrosion mechanism of the Mg–Y alloy was not been clearly revealed, which exhibited higher corrosion resistance than commercially pure Mg. Previous investigations reported that the distribution of the RE-phase determines the corrosion resistance of the Mg–RE alloys [31,32]. At a low

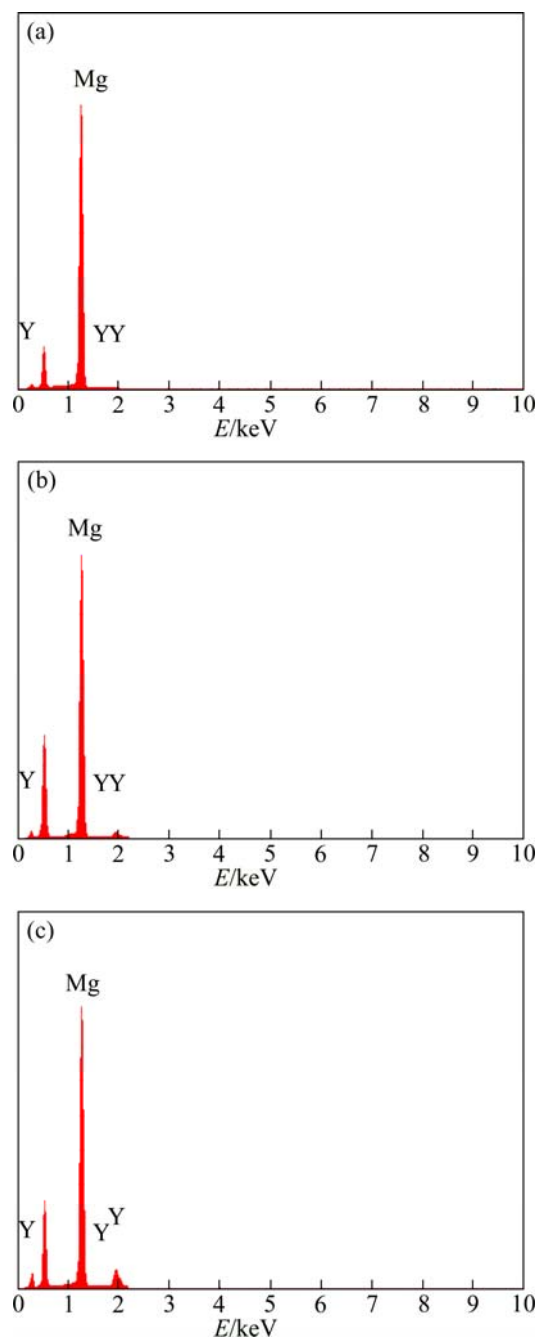


Fig. 7 EDS analysis on surfaces of Mg–Y alloys after removing corrosion products: (a) Mg–0.25Y; (b) Mg–8Y; (c) Mg–15Y

volume fraction, the RE-phase serves as a galvanic cathode and accelerates the corrosion process of the α -phase, whereas at a large volume fraction it acts as an anodic barrier and the overall corrosion diminishes. Apart from the microstructure, the composition of the corrosion layer may improve the corrosion resistance. For instance, KRISTA et al [33] observed that yttrium components formed a continuous skeletal structure in the oxide layer of magnesium alloy, whose passivating properties were much better than those of the $Mg(OH)_2$ and MgO layers.

3.4 Corrosion products

The XRD patterns of corrosion products on the surface of three samples after immersion are shown in Fig. 8. From Fig. 8, it was found that the corrosion products mainly consisted of $\text{Mg}(\text{OH})_2$ and $\text{Mg}_2(\text{OH})_3\text{Cl}\cdot 4\text{H}_2\text{O}$. The Cl^- ion in the solution promoted the corrosion of samples, and generated more thermodynamically stable corrosion products $\text{Mg}(\text{OH})_2$ by the following equations [34]:

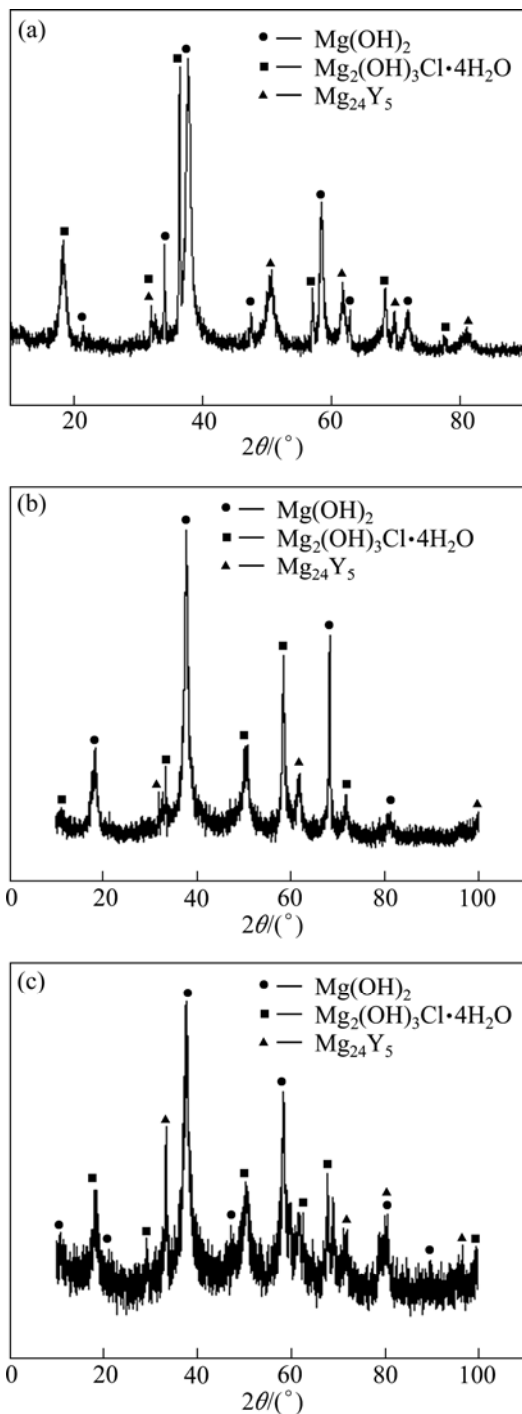
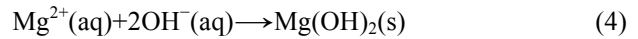


Fig. 8 XRD patterns of corrosion products: (a) Mg-0.25Y; (b) Mg-8Y; (c) Mg-15Y



The reaction occurred in the solution because of the existence of Cl^- according to [35]



However, Mg_{24}Y_5 phase was also found in the corrosion products, and this can be explained that the Mg_{24}Y_5 phase fell off from the alloy and left in the corrosion products. And this also indicated that the Mg_{24}Y_5 phase was too stable to be corroded in the NaCl solution. This phenomenon could be in accordance with the explanation in Fig. 7.

3.5 Electrochemical results

3.5.1 Polarization curves

The potentiodynamic polarization curves of Mg-Y alloys are shown in Fig. 9. From Fig. 9, the corrosion potential shifted positively, approximately from -1.605 V to -1.580 V and the corrosion current density increased with the increase of yttrium addition. Judged from the cathodic branches, the addition of yttrium obviously activated the cathodic reaction. However, the influence of yttrium on the anodic reaction was not as obvious as that on the cathodic reaction, as indicated in Fig. 9. But, the anodic branch presented an obvious step with the increase of yttrium addition, which indicated that the yttrium could increase the stability of corrosion film on the sample surface. Consequently, the corrosion potential of Mg-Y alloys was improved in virtue of the addition of yttrium.

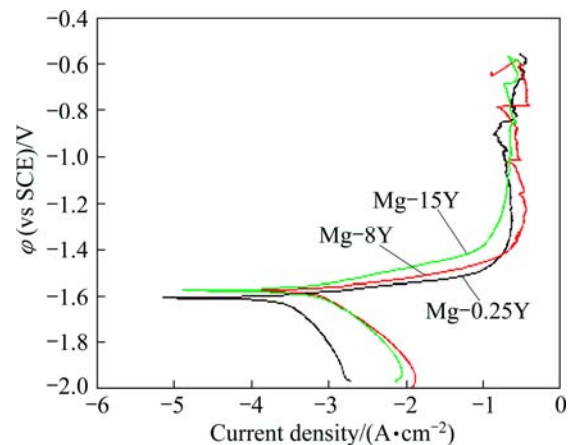


Fig. 9 Polarization curves of Mg-Y alloys in 3.5% NaCl solution

It could be found that the cathodic sides of Mg-Y alloys were driven with hydrogen evolution reaction. The corrosion current density gradually decreased with potential moving toward φ_{corr} , implying that the hydrogen evolution rate diminished. After the corrosion

potential reached φ_{corr} , the curves entered into the anodic region. The corrosion current density increased slowly with the increase of anodic potential. When the corrosion potential reached a certain value, the pitting corrosion occurred. Once the anodic potential reached the corrosion potential of the film breakdown, the oxide film on the surface fractured and the magnesium substrates were corroded quickly [36]. The pitting corrosion was not visible in Fig. 2 because the pitting potential (φ_{pit}) was very close to φ_{corr} . Consequently, it was expected that these alloys suffered the pitting attack immediately after their immersion in 3.5% NaCl solution at the open circuit potential. However, the current densities of the cathodic branch and the growth of corrosion products on the material surface were quite high, suggesting that the general corrosion attack acted as the main mechanism of degradation [37]. As discussed above, yttrium addition to the magnesium alloy facilitated the formation of less cathodic Y-containing phase. The electrochemical polarization curve results confirmed the change of microstructure of Mg–Y alloys.

3.5.2 EIS analysis

The corrosion current density decreased with the increasing of yttrium addition. So the content of Y had influence on the corrosion resistance of Mg–Y alloys. The traditional Tafel equation can not be simply used to describe the polarization behaviour of Mg–Y alloys. As a result, the results from polarization curves could not perfectly distinguish the influence of the addition of yttrium on the corrosion rate of Mg–Y alloys. However, the EIS measurements can better estimate the corrosion behavior of magnesium alloys together with hydrogen evolution test [38].

The EIS measurements of Mg–Y alloys after different exposure time in 3.5% NaCl solution were conducted and the results are shown in Figs. 10 and 11. Figure 10 exhibits three capacitive loops for the three alloys, indicating that the three alloys had the same corrosion mechanism in 3.5% NaCl solution. The Nyquist plot for the samples consisted of three loops, high frequency capacitive loop, medium frequency capacitive loop and short low frequency inductive loop. Their diameters were dependent on the composition and, possibly, on the microstructure of tested alloys. At low frequencies for the three samples, the Nyquist plots revealed an inductive behavior, and some points had

negative values (omitted from the plots) because the disperse points at low frequencies might be due to the high activity of magnesium alloys. Sometimes these arcs were less evident than the other parts in the Nyquist plots. According to ZHANG and CAO [39], the low frequency inductive loop is attributed to the corrosion nucleation at the initiation stage of localized corrosion. At high frequency for the three samples, the points of the Nyquist plots scattered chaos which might be caused by the beginning of the corrosion and the formation of corrosion products on the surfaces. It should be noticed in Fig. 11 that most of the phase angles exceeded 45° , and the maximum phase angle of high frequency capacitive arcs exceeded 70° in Bode plots. So, the uneven current distribution in these EIS tests could be considered to be minimized. According to the Bode plot of $|Z|$ vs frequency, it was found that the $|Z|$ value increased in the order of Mg–8Y, Mg–15Y and Mg–0.25Y.

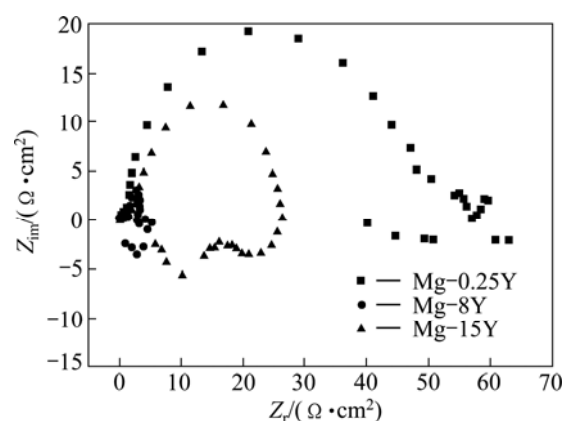


Fig. 10 Nyquist plot of Mg–Y alloys

Based upon the equivalent circuit given in Fig. 12, the measured impedance data were analyzed by using a complex non-linear least squares (CNLS) fitting method [40,41]. The change of relevant fitted values of the circuit elements are presented in Table 2 and Fig. 13. It was observed from Table 2 and Fig. 13 that the impedance value of (R_c+R_t) increased in the initial immersion time, while R_p and L decreased. This indicated that at the first stage of immersion, pitting corrosion became more active as more defective pores were filled with solution and more corrosion products accumulated in the defective pores. When the immersion

Table 2 Parameters of equivalent circuit for Mg–Y alloys

Sample	$R_c/$ ($\Omega\cdot\text{cm}^2$)	$R_p/$ ($\Omega\cdot\text{cm}^2$)	$R_b/$ ($\Omega\cdot\text{cm}^2$)	$R_t/$ ($\Omega\cdot\text{cm}^2$)	$R_h/$ ($\Omega\cdot\text{cm}^2$)	$\text{CPE}_t/$ ($\mu\text{F}\cdot\text{cm}^{-2}$)	$\text{CPE}_b/$ ($\mu\text{F}\cdot\text{cm}^{-2}$)	n	$L/$ ($\text{H}\cdot\text{cm}^{-2}$)	Q
Mg–0.25Y	0.328	30.80	32.99	11.57	9.310	6.408×10^{-6}	0.002269	0.8887	59.66	2.531×10^{-5}
Mg–8Y	0.2985	7.314	1×10^{-7}	13.637	3.315×10^{-5}	1.661×10^{-6}	3.624×10^{-8}	0.8888	32.74	4.00×10^{-5}
Mg–15Y	0.9841	3.86	12.73	16.28	0.4862	8.608×10^{-6}	1.43×10^{-5}	0.8885	31.83	1.538×10^{-5}

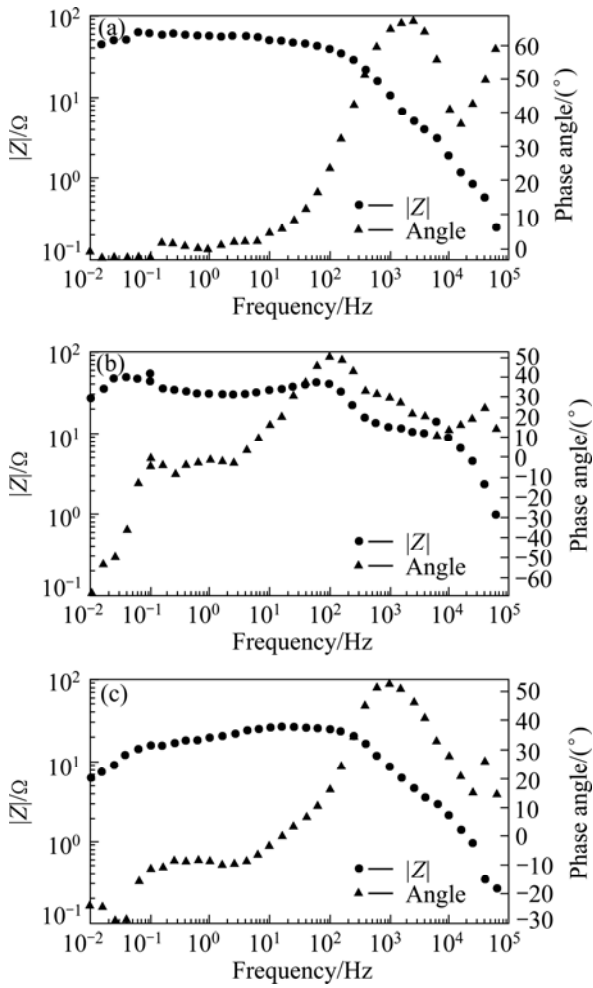


Fig. 11 Bode plots of samples: (a) Mg-0.25Y; (b) Mg-8Y; (c) Mg-15Y

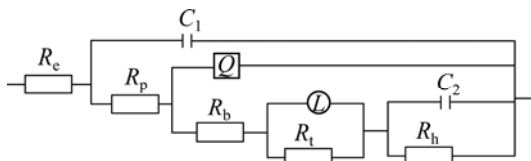


Fig. 12 Equivalent circuit of EIS plots

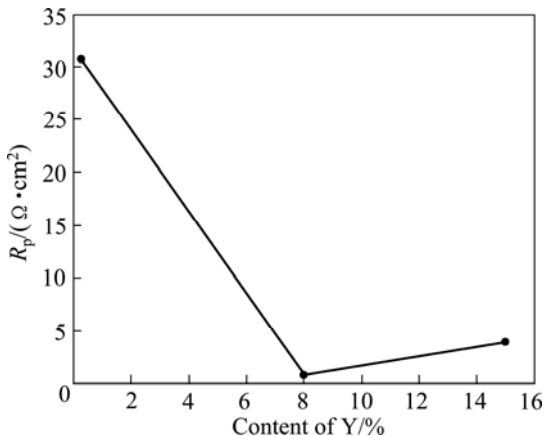


Fig. 13 Changes of R_p with content of Y in Mg-Y alloys

time was longer than a certain time, the contact between the intermetallic $Mg_{24}Y_5$ and the solution came to a fixed value due to the balance of the inward growth and active dissolution of the defects and Cl^- ion incorporated out the film, which accorded with the results studied by TAO et al [42].

The detailed interpretation of the EIS data was carried out by numerical fitting of the experimental data, as shown in Table 2. For fitting the experimental impedance results, various trials were done using the equivalent circuits. The best fitting parameters and lowest errors were obtained with the Voigt circuit described in Fig. 12. The capacitance was replaced by the so-called constant phase angle element. The presence of CPE had been explained by dispersion effects that could be caused by microscopic roughness of surface [43]. The high frequency time constant was assigned to the response of the passive film, whereas the time constant at lower frequencies was correlated with the charge transfer processes and electrical double layer capacitance at the surface of contact between the base metal and the passive film. The change of R_p with addition of yttrium is shown in Fig. 13. It could be observed that R_p decreased when the addition of yttrium was below 8% and then increased when the addition of yttrium was above 8%, up to 15%.

4 Conclusions

- 1) The microstructure of as-cast Mg-Y alloys consisted of primary α -Mg and $Mg_{24}Y_5$ phase. The increase of yttrium content in the alloys reduced the activity of pure Mg in 3.5% NaCl solution, and the corrosion resistance was exclusively attributed to the presence of network of eutectic aggregate with higher Y content, which hindered the advance of the corrosion attack.
- 2) Mg-Y alloys consisted of a dual phase structure of α and $Mg_{24}Y_5$ phase, resulting in corrosion attack of the three Mg-Y alloys at the α -Mg/ $Mg_{24}Y_5$ intermetallic compounds interfaces, by means of the formation of galvanic couples.
- 3) The corrosion rate increased with increasing Y addition because of the increment of $Mg_{24}Y_5$ intermetallic amounts.
- 4) The sequence of corrosion initiation and propagation involved pitting initially adjacent to the $Mg_{24}Y_5$ phase, followed by deep attack at the Y-rich regions, and pitting within the α -Mg phase.
- 5) The corrosion products mainly consisted of $Mg(OH)_2$ and $Mg_2(OH)_3Cl \cdot 4H_2O$.

Acknowledgements

This work was supported by Beijing Engineering

Research Center for Advanced Manufacturing and Evaluation of Special Vehicle Parts which is jointly built by Beijing North Vehicle Group Corporation and University of Science and Technology Beijing. We also gratefully acknowledge the selfless help on alloy SEM observations by Dr. Jian-hua BIAN, from University of Science and Technology Beijing.

References

- [1] SHAW B A. Corrosion resistance of magnesium alloys [M]// KORB L J. ASM Handbook. Vol. 13A. Corrosion. 9th ed. Metals Park: ASM International Handbook Committee, 2003: 692.
- [2] SONG G, ATRENS A. Understanding magnesium corrosion—A framework for improved alloy performance [J]. *Advanced Engineering Materials*, 2003, 5: 837–858.
- [3] SONG G. Recent progress in corrosion and protection of magnesium alloys [J]. *Advanced Engineering Materials*, 2005, 7: 563–586.
- [4] MAJUMDAR J D, GALUN R, MORDIKE B, MANNA I. Effect of laser surface melting on corrosion and water resistance of a commercial magnesium alloy [J]. *Materials Science and Engineering A*, 2003, 361: 119–129.
- [5] ROSALBINO F, ANGELINI E, NEGRI S D, SACCONI A, DELFINO S. Effect of erbium addition on the corrosion behavior of Mg–Al alloys [J]. *Intermetallics*, 2005, 13: 55–60.
- [6] LIU W, CAO F, ZHONG L, ZHENG L, JIA B, ZHANG Z, ZHANG J. Influence of rare earth element Ce and La addition on corrosion behavior of AZ91 magnesium alloy [J]. *Materials and Corrosion*, 2009, 60: 795–803.
- [7] SONG Y L, LIU Y H, YU S R, ZHU X Y, WANG S H. Effect of neodymium on microstructure and corrosion resistance of AZ91 magnesium alloy [J]. *Journal of Materials Science*, 2007, 42: 4435–4440.
- [8] PINTO R, CARMEZIM M J, FERREIRA M G S, MONTEMOR M F. A two-step surface treatment, combining anodisation and silanisation, for improved corrosion protection of the Mg alloy WE54 [J]. *Progress in Organic Coatings*, 2010, 69: 143–149.
- [9] GUO L F, YUE T M, MAN H C. Excimer laser surface treatment of magnesium alloy WE43 for corrosion resistance improvement [J]. *Journal of Materials Science*, 2005, 40: 3531–3533.
- [10] ZHANG Xin, ZHANG Kui, LI Xing-gang, Wang Cong, LI Hong-wei, WANG Chang-shun, DENG Xia. Corrosion and electrochemical behavior of as-cast Mg–5Y–7Gd–1Nd–0.5Zr magnesium alloys in 5% NaCl aqueous solution [J]. *Progress in Natural Science: Materials International*, 2011, 21: 314–321.
- [11] BEN-HAMU G, ELIEZER D, SHIN K S, COHEN S. The relationship between microstructure and corrosion behaviour of Mg–Y–RE–Zr alloys [J]. *Journal of Alloys and Compounds*, 2007, 431: 269–276.
- [12] ZHANG E L, He W W, DU H. Microstructure, mechanical properties and corrosion properties of Mg–Zn–Y alloys with low Zn content [J]. *Materials Science and Engineering A*, 2008, 488: 102–111.
- [13] ROKHLIN L L. *Magnesium alloys containing rare earth metals* [M]. London, UK: Taylor & Francis, 2003.
- [14] SOCIJUSZ-PODOSEK M, LITYŃSKA L. Effect of yttrium on structure and mechanical properties of Mg alloys [J]. *Materials Chemistry and Physics*, 2003, 80: 472–475.
- [15] ZHANG M X, KELLY P M. Morphology and crystallography of Mg₂₄Y₅ precipitate in Mg–Y alloy [J]. *Scripta Materialia*, 2003, 48: 379–384.
- [16] LIU M, SCHMUTZ P, UGGOWITZER P J, SONG G, ATRENS A. The influence of yttrium (Y) on the corrosion of Mg–Y binary alloys [J]. *Corrosion Science*, 2010, 52: 3687–3701.
- [17] SUDHOLZ A D, GUSIEVA K, CHEN X B, MUDDLE B C, GIBSON M A, BIRBILIS N. Electrochemical behaviour and corrosion of Mg–Y alloys [J]. *Corrosion Science*, 2011, 53: 2277–2282.
- [18] QIU D, ZHANG M X, KELLY P M. Crystallography of heterogeneous nucleation of Mg grains on Al₂Y nucleation particles in an Mg–10 wt.% Y alloy [J]. *Scripta Materials*, 2009, 61: 312–315.
- [19] MILLER P L, SHAW B A, WENDT R G, MOSHIER W C. Assessing the corrosion resistance of nonequilibrium magnesium–yttrium alloys [J]. *Corrosion*, 1995, 52: 922–931.
- [20] DAVENPORT A J, PADOVANI C, CONNOLLY B J, STEVENS N P C, BEALE T A W, GROSO A, STAMPANONI M, GROSO A, STAMPANONI M. Synchrotron X-ray microtomography study of the role of Y in corrosion of magnesium alloy WE43 [J]. *Electrochemical and Solid-State Letters*, 2007, 10: C5–C8.
- [21] LI Y J, ZHANG K, LI X G, MA M L. Evolution of microstructure and mechanical properties of Mg–5Y–5Gd–xNd–0.5Zr magnesium alloys at different states [J]. *Rare Metals*, 2010, 29: 317–322.
- [22] ZHAO Ming-chun, LIU Ming, SONG Guang-ling, ATRENS A. Influence of the β -phase morphology on the corrosion of the Mg alloy AZ91 [J]. *Corrosion Science*, 2008, 50: 1939–1953.
- [23] COY A E, VIEJO F, SKELDON P, THOMPSON G E. Susceptibility of rare-earth-magnesium alloys to micro-galvanic corrosion [J]. *Corrosion Science*, 2010, 52: 3896–3906.
- [24] ZHANG X, ZHANG K, DENG X, LI H W, LI Y J, MA M L, LI N, WANG Y L. Corrosion behavior of Mg–Y alloy in NaCl aqueous solution [J]. *Progress in Natural Science: Materials International*, 2012, 22(2): 169–174.
- [25] RUGGERI R T, BECK T R. An analysis of mass transfer in filiform corrosion [J]. *Corrosion*, 1983, 39: 452–465.
- [26] SCHMUTZ P, GUILLAUMIN V, LILLARD R S, LILLARD J A, FRANKEL G S. Influence of dichromate ions on corrosion processes on pure magnesium [J]. *J Electrochem Soc*, 2003, 150: B99–B110.
- [27] WANG Qiang, LIU Yao-hui, FANG Shi-jie, SONG Yu-lai, ZHANG Da-wei, ZHANG Li-na, LI Chun-fang. Evaluating the improvement of corrosion residual strength by adding 1.0wt.% yttrium into an AZ91D magnesium alloy [J]. *Materials Characterization*, 2010, 61: 674–682.
- [28] CHEN Jian, WANG Jian-qiu, HAN En-hou, DONG Jun-hua, KE Wei. AC impedance spectroscopy study of the corrosion behavior of an AZ91D magnesium alloy in 0.1 M sodium sulfate solution [J]. *Electrochim Acta*, 2007, 52: 3299–3309.
- [29] NEIL W C, FORSYTH M, HOWLETT P C, HUTCHINSON C R, HINTON B R W. Corrosion of magnesium alloy ZE41—The role of microstructural features [J]. *Corrosion Science*, 2009, 51: 387–394.
- [30] BAUMGÄRTNER M, KAESCHE H. Aluminum pitting in chloride solutions: Morphology and pit growth kinetics [J]. *Corrosion Science*, 1990, 31: 231–236.
- [31] BIRBILIS N, EASTON M A, SUDHLOZ A D, ZHU S M, GIBSON M A. On the corrosion of binary magnesium-rare-earth alloys [J]. *Corrosion Science*, 2009, 51: 683–689.
- [32] ZUCCHI F, GRASSI V, FRIGNANI A. Electrochemical behaviour of a magnesium alloy containing rare earth elements [J]. *Journal of Applied Electrochemistry*, 2006, 36: 195–204.
- [33] HEIDERSBACH K L. An evaluation of the corrosion performance of magnesium-yttrium and yttrium-magnesium nonequilibrium alloys [D]. The Pennsylvania State University, 1998.
- [34] BARIL G, GALICIA G, DESLOUIS C, PEBERE N, TRIBOLLET B, VIVIER V. An impedance investigation of the mechanism of pure magnesium corrosion in sodium sulphate solution [J]. *Journal of the Electrochemical Society*, 2007, 154: C108–C113.
- [35] SONG G, ATRENS A, DARGUSCH M. Influence of microstructure

- on the corrosion of diecast AZ91D [J]. Corrosion Science, 1999, 41: 249–273.
- [36] SONG Ying-wei, SHAN Da-yong, CHEN Rong-shi, HAN En-hou. Corrosion characterization of Mg–8Li alloy in NaCl solution [J]. Corrosion Science, 2009, 51: 1087–1094.
- [37] PARDO A, MERINO M C, COY A E, ARRABAL R, VIEJO F, MATYKINA E. Corrosion behaviour of magnesium/aluminium alloys in 3.5wt.% NaCl [J]. Corrosion Science, 2008, 50: 823–834.
- [38] LIU Wen-juan, CAO Fa-he, CHANG Lin-rong, ZHANG Zhao, ZHANG Jian-qing. Effect of rare earth element Ce and La on corrosion behavior of AM60 magnesium alloy [J]. Corrosion Science, 2009, 51: 1334–1343.
- [39] ZHANG Jian-qing, CAO Chu-nan. Introduction of electrochemical impedance spectroscopy [J]. Beijing: Science Press, 2002. (in Chinese)
- [40] BAE J S, PYUN S I. An AC-impedance study of li-Al₂O₃ composite solid-electrolyte [J]. Journal of Materials Science Letters, 1994, 13: 573–576.
- [41] SADKOWSKI A. CNLS fits and Kramers–Kronig validation of resonant EIS data [J]. Journal of Electroanalytical Chemistry, 2004, 573: 241–253.
- [42] TAO Yong-shan, XIONG Tian-ying, SUN Chao, KONG Ling-yan, CUI Xin-yu, LI Tie-fan, SONG Guang-ling. Microstructure and corrosion performance of a cold sprayed aluminium coating on AZ91D magnesium alloy [J]. Corrosion Science, 2010, 52: 3191–3197.
- [43] KIRKLAND N T, LESPAGNOL J, BIRBILIS N, STAIGER M P. A survey of bio-corrosion rates of magnesium alloys [J]. Corrosion Science, 2010, 52: 287–291.

Mg–Y 镁合金在 3.5% NaCl 溶液中的腐蚀和电化学行为

张新^{1,2,3}, 李永军¹, 张奎¹, 王长顺^{2,3}, 李宏伟^{2,3}, 马鸣龙¹, 张宝东^{2,3}

1. 北京有色金属研究总院 有色金属材料制备加工国家重点实验室, 北京 100088;
2. 北京市特种车辆部件制造与评估工程技术研究中心, 北京 100072;
3. 北京北方车辆集团有限公司工艺技术中心, 北京 100072

摘要: 在 3.5% NaCl 水溶液中通过浸泡、形貌观察和电化学测试研究 Mg–Y 镁合金的腐蚀性能。结果表明, 随着 Y 含量的增加, Mg–Y 合金的腐蚀电位增加。由于第二相 Mg₂₄Y₅ 的增加, Mg–Y 镁合金的腐蚀速率随着 Y 含量的增加而逐渐增加。在腐蚀过程中, 随着腐蚀时间的延长, 合金的腐蚀程度逐渐严重。Mg–0.25Y 和 Mg–(8, 15)Y 合金的腐蚀形貌分别为均匀腐蚀和点蚀。Mg–Y 镁合金的腐蚀产物主要为 Mg(OH)₂ 和 Mg₂(OH)₃Cl·4H₂O。

关键词: Mg–Y 合金; 极化曲线; 点蚀; 腐蚀产物

(Edited by Sai-qian YUAN)